

Effect of External Normal and Parallel Electric Fields on 180° Ferroelectric Domain Walls in PbTiO_3

Arzhang Angoshtari and Arash Yavari*

School of Civil and Environmental Engineering, Georgia Institute of Technology, Atlanta, GA 30332.

(Dated: February 16, 2022)

We impose uniform electric fields both parallel and normal to 180° ferroelectric domain walls in PbTiO_3 and obtain the equilibrium structures using the method of anharmonic lattice statics. In addition to Ti-centered and Pb-centered perfect domain walls, we also consider Ti-centered domain walls with oxygen vacancies. We observe that electric field can increase the thickness of the domain wall considerably. We also observe that increasing the magnitude of electric field we reach a critical electric field E^c ; for $E > E^c$ there is no local equilibrium configuration. Therefore, E^c can be considered as an estimate of the threshold field E_h for domain wall motion. Our numerical results show that Oxygen vacancies decrease the value of E^c . As the defective domain walls are thicker than perfect walls, this result is in agreement with the recent experimental observations and continuum calculations that show thicker domain walls have lower threshold fields.

I. INTRODUCTION

Ferroelectric materials have been used in many important applications such as high strain actuators, electro-optical systems, non-volatile and high density memories, etc.^{1,2}. The properties of domain walls in ferroelectric materials including their structure, thickness, and mobility are important parameters as they determine the performance of devices that use these materials³.

Theoretical calculations have predicted that ferroelectric domain walls are atomically sharp and their thickness is about a few angstroms⁴⁻⁷. However, experimental measurements show the existence of domain walls with thicknesses of a few micrometers^{8,9}. It has been observed that such broadening of domain walls is due to the presence of extrinsic defects, charged walls, and surfaces¹⁰. Shilo *et al.*¹¹ used atomic force microscopy to measure the surface profile close to emerging domain walls in PbTiO_3 and then fitted it to the soliton-type solution of GLD theory. They measured wall widths of 1.5nm and 4nm and observed a wide scatter in wall widths. They suggested that the presence of point defects is responsible for such wide variations. Lee *et al.*¹² proposed a continuum model to investigate this proposal and reproduced the experimentally observed range of wall widths with their model. They mentioned that the interaction between the order parameter and point defects and interaction of point defects with each other are two important interactions that should be considered properly in such modelings. Jia *et al.*³ investigated the cation-oxygen dipoles near 180° domain walls in $\text{PbZr}_{0.2}\text{Ti}_{0.8}\text{O}_3$ thin films. They measured the width and dipole distortion across domain walls using the negative spherical-aberration imaging technique in an aberration-corrected transmission electron microscope and observed a large difference in atomic details between charged and uncharged domain walls.

External electric field can cause the motion of ferroelectric domain walls if the magnitude of the field reaches the threshold field E_h for wall motion, i.e., the field at which a domain wall begins to move after overcoming the intrinsic Peierls friction of the ferroelectric lattice¹⁰. It was

observed that threshold fields that are predicted via thermodynamic calculations are usually much greater than the experimental values. For example, Bandyopadhyay and Ray¹³ predicted an upper limit for E_h of LiNbO_3 to be 30000kV/cm but experimental observations show that the threshold field for wall motion can be less than 15kV/cm . Choudhury *et al.*¹⁰ suggested that the reason for such large differences between theoretical and experimental values of E_h is broadening of the domain walls. Using microscopic phase-field modeling, they show that the threshold field for moving an antiparallel ferroelectric domain wall dramatically drops by two or three orders of magnitude if the wall was diffused by only about $1-2\text{nm}$. Su and Landis¹⁴ developed a continuum thermodynamics framework to model the evolution of ferroelectric domain structures and investigated the fields near 90° and 180° domain walls and the electromechanical pinning strength of an array of line charges on these domain walls.

In this work, we investigate the effect of external electric field (E) on the perfect and defective 180° domain walls in PbTiO_3 using the method of anharmonic lattice statics. We consider both Pb-centered and Ti-centered perfect domain walls and also defective domain walls with oxygen vacancies. In agreement with experimental results, our calculations show that such defective domain walls are thicker than perfect walls¹⁸. By increasing E we reach a critical value E^c such that for $E > E^c$ the lattice statics iterations do not converge. Therefore, this critical value can be considered as a lower bound for the threshold field for wall motion.

This paper is organized as follows. In §II, we explain the geometry of the perfect and defective domain walls that we use throughout this work. In §III, we describe the method of analysis used in our calculations. Our numerical results are presented in §IV. The paper ends with some concluding remarks in §V.

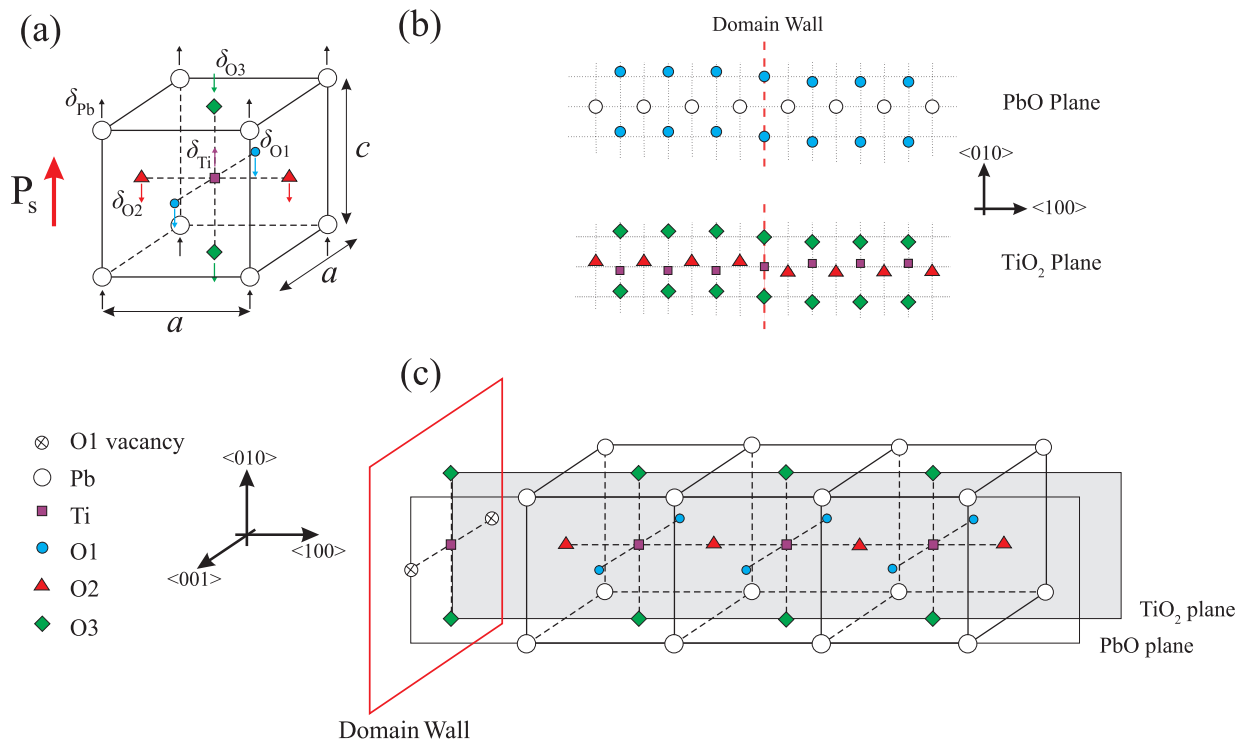


FIG. 1: (a) The relaxed configuration of the unit cell of PbTiO_3 . a and c are the tetragonal lattice parameters. Note that O1, O2, and O3 refer to oxygen atoms located on (001), (100), and (010)-planes, respectively. δ denotes the y-displacements of the atoms from their centrosymmetric positions and arrows near each atom denote the direction of these displacements. (b) The geometry of a perfect Ti-centered 180° domain wall. (c) The geometry of an O1-defective 180° domain wall. Note that Pb-centered domain walls with oxygen vacancies are not stable.

II. FERROELECTRIC DOMAIN WALLS

Due to the relative displacements between the center of the positive and negative charges, each unit cell of a ferroelectric crystal has a net polarization below its Curie temperature. Fig.1(a) shows the relaxed unit cell of tetragonal PbTiO_3 . In this work, we consider 180° domain walls in PbTiO_3 parallel to a (100)-plane. These domain walls are two dimensional defects across which the direction of the polarization vector switches. There are two types of perfect 180° domain walls in PbTiO_3 : Pb-centered and Ti-centered domain walls. Fig.1(b) shows the geometry of a Ti-centered domain wall.

In addition to perfect domain walls, we also consider 180° domain walls with oxygen vacancies. It is known that oxygen vacancies tend to move toward domain walls and pin them^{15–17}. Therefore, we study domain walls with oxygen vacancies sitting on them. In order to be able to obtain a solution, we need to consider periodically arranged vacancies on the domain walls. Although in reality oxygen vacancies have lower densities, our results with the current assumption can still provide important insights on the effect of oxygen vacancies on 180° domain walls. Depending on which oxygen in the PbTiO_3 unit cell sits on the domain wall, there would be three types of defective domain walls: (i) O2-defective,

(ii) O1-defective, and (iii) O3-defective. Fig.1(c) shows an O1-defective domain wall. Note that O1- and O3-defective domain walls are Ti-centered while O2-defective domain wall is Pb-centered. It has been observed that O2-defective domain walls are not stable^{15,18}, i.e., the lattice statics iterations do not converge. Thus, we consider O1- and O3-defective domain walls in the following.

Let x , y , and z denote coordinates along the $\langle 100 \rangle$, $\langle 010 \rangle$, and $\langle 001 \rangle$ -directions, respectively. We assume a 1D symmetry reduction, which means that all the atoms with the same x -coordinates have the same displacements. Therefore, we partition the 3D lattice \mathcal{L} as $\mathcal{L} = \bigsqcup_I \bigsqcup_{\alpha \in \mathbb{Z}} \mathcal{L}_{I\alpha}$, where $\mathcal{L}_{I\alpha}$ and \mathbb{Z} are 2D equivalence classes parallel to the (100) plane and the set of integers, respectively. $j = J\beta$ is the atom in the β th equivalence class of the J th sublattice. See^{19,20} for more details on the symmetry reduction.

III. METHOD OF CALCULATION

We apply a uniform electric field on 180° domain walls and obtain the equilibrium structure using the method of anharmonic lattice statics¹⁹. We use a shell potential for PbTiO_3 ²¹ for modeling the atomic interactions. Each ion is represented by a core and a massless shell in this potential. Let \mathcal{L} denote the collection of cores and shells,

$i \in \mathcal{L}$ denotes a core or a shell in \mathcal{L} , and $\{\mathbf{x}^i\}_{i \in \mathcal{L}}$ represents the current position of cores and shells. In this shell potential, three different energies are assumed to exist due to the interactions of cores and shells: $\mathcal{E}_{\text{short}}$, $\mathcal{E}_{\text{long}}$, and $\mathcal{E}_{\text{core-shell}}$. $\mathcal{E}_{\text{short}}(\{\mathbf{x}^i\}_{i \in \mathcal{L}})$ denotes the energy of short range interactions, which are assumed to be only between Pb-O, Ti-O, and O-O shells. The short range interactions are described by the Rydberg potential of the form $(A + Br) \exp(-r/C)$, where A, B, and C are potential parameters and r is the distance between interacting elements. $\mathcal{E}_{\text{long}}(\{\mathbf{x}^i\}_{i \in \mathcal{L}})$ denotes the Coulombic interactions between the core and shell of each ion with the cores and shells of all the other ions. For calculating the classical Coulombic energy and force, we use the damped Wolf method²². Finally, $\mathcal{E}_{\text{core-shell}}(\{\mathbf{x}^i\}_{i \in \mathcal{L}})$ represents the interaction of core and shell of an atom and is assumed to be an anharmonic spring of the form $(1/2)k_2r^2 + (1/24)k_4r^4$, where k_2 and k_4 are constants. The total static energy is written as

$$\mathcal{E}(\{\mathbf{x}^i\}_{i \in \mathcal{L}}) = \mathcal{E}_{\text{short}}(\{\mathbf{x}^i\}_{i \in \mathcal{L}}) + \mathcal{E}_{\text{long}}(\{\mathbf{x}^i\}_{i \in \mathcal{L}}) + \mathcal{E}_{\text{core-shell}}(\{\mathbf{x}^i\}_{i \in \mathcal{L}}). \quad (1)$$

Note that all the calculations are done for absolute zero temperature. At this temperature PbTiO₃ has a tetragonal unit cell with lattice parameters $a = 3.843 \text{ \AA}$ and $c = 1.08a$ ²¹.

Assume that a uniform electric field $\mathbf{E} = (E_x, E_y, E_z)$ is applied to a collection of atoms. Then for the relaxed configuration $\mathcal{B} = \{\mathbf{x}^i\}_{i \in \mathcal{L}} \subset \mathbb{R}^3$, we have

$$\frac{\partial \mathcal{E}}{\partial \mathbf{x}^i} + q_i \mathbf{E} = \mathbf{0} \quad \forall i \in \mathcal{L}, \quad (2)$$

where q_i denotes the charge of the i th particle (core or shell). To obtain the solution of the above problem, we utilize the Newton method. Having a configuration \mathcal{B}^k the next configuration \mathcal{B}^{k+1} is calculated from the current configuration \mathcal{B}^k as: $\mathcal{B}^{k+1} = \mathcal{B}^k + \tilde{\delta}^k$, where

$$\tilde{\delta}^k = -\mathbf{H}^{-1}(\mathcal{B}^k) \cdot \nabla \mathcal{E}(\mathcal{B}^k), \quad (3)$$

with \mathbf{H} denoting the Hessian matrix. The calculation of the Hessian becomes inefficient as the size of the problem increases and hence we use the quasi-Newton method. This method uses the Broyden-Fletcher-Goldfarb-Shanno (BFGS) algorithm to approximate the inverse of the Hessian²³ instead of the direct calculation of the Hessian at each iteration. We start from a positive-definite matrix and use the BFGS algorithm to update the Hessian at each iteration as follows:

$$\mathbf{C}^{i+1} = \mathbf{C}^i + \frac{\tilde{\delta}^k \otimes \tilde{\delta}^k}{(\tilde{\delta}^k)^\top \cdot \Delta} - \frac{(\mathbf{C}^i \cdot \Delta) \otimes (\mathbf{C}^i \cdot \Delta)}{\Delta^\top \cdot \mathbf{C}^i \cdot \Delta} + (\Delta^\top \cdot \mathbf{C}^i \cdot \Delta) \mathbf{u} \otimes \mathbf{u}, \quad (4)$$

where $\mathbf{C}^i = (\mathbf{H}^i)^{-1}$, $\Delta = \nabla \mathcal{E}^{i+1} - \nabla \mathcal{E}^i$, and

$$\mathbf{u} = \frac{\tilde{\delta}^k}{(\tilde{\delta}^k)^\top \cdot \Delta} - \frac{\mathbf{C}^i \cdot \Delta}{\Delta^\top \cdot \mathbf{C}^i \cdot \Delta}. \quad (5)$$

Calculating \mathbf{C}^{i+1} , one then should use \mathbf{C}^{i+1} instead of \mathbf{H}^{-1} to update the current configuration. If \mathbf{C}^{i+1} is a poor approximation, then one may need to perform a linear search to refine \mathcal{B}^{k+1} before starting the next iteration²³.

In the presence of oxygen vacancies on the domain wall, one needs to consider charge redistribution between some ions. To model an oxygen vacancy using a shell potential, we remove the core and shell of the oxygen atom and because we assume a charge neutral oxygen vacancy, there will be a charge redistribution in the neighboring shells¹⁸. It is known that charge redistribution is highly localized and hence in our calculations we equally distribute the charge $\Delta Q = Q_s + Q_c$, where Q_s and Q_c are oxygen shell and core charges, between the (fourteen) first nearest neighbors of each oxygen vacancy.

To obtain the equilibrium configuration under an external electric field we need to start from an appropriate initial configuration. This initial configuration for perfect and defective domain walls is the equilibrium configuration of these domain walls under zero electric field (see^{6,18} for discussions on how to calculate these configurations). As we mentioned earlier, we assume a 1D symmetry reduction for the lattice and hence as is shown in Fig.2, our computational box (CB) consists of a row of unit cells perpendicular to the domain wall. In this figure, the shaded region is the computational box. Note that because in general there is no symmetry in the problem, we need to relax all the atoms inside the CB. For removing the rigid body translation freedom of the atoms, one should fix the core of an atom and relax the other atoms. We fix Pb-core (Ti-core) of an atom located on the domain wall in Pb-centered (Ti-centered) domain walls. Thus, if there are M unit cells in the CB, we would have $30M - 3$ variables in our calculations. We should mention that to investigate the effect of the size of CB in the domain wall plane, we consider CBs with one, four, and sixteen unit cells in the domain wall plane and therefore the number of the unit cells in CB in each case is M , $4M$, and $16M$, respectively. We observe that the final relaxed structure does not depend on the size of CB in the domain wall plane. This suggests that the symmetry reduction that we use in our calculations is a reasonable assumption for this problem.

Note that we consider a finite number of unit cells in the CB and do not assume any periodicity condition in our calculations. This means that we need to impose some proper boundary conditions to take into account the effect of the atoms located outside of CB. To this end, we rigidly move the unit cells outside of CB with displacements equal to those of the first or last unit cell of the CB (the unit cell on the boundary of the CB that is closer to the unit cell outside of the CB). This is a natural

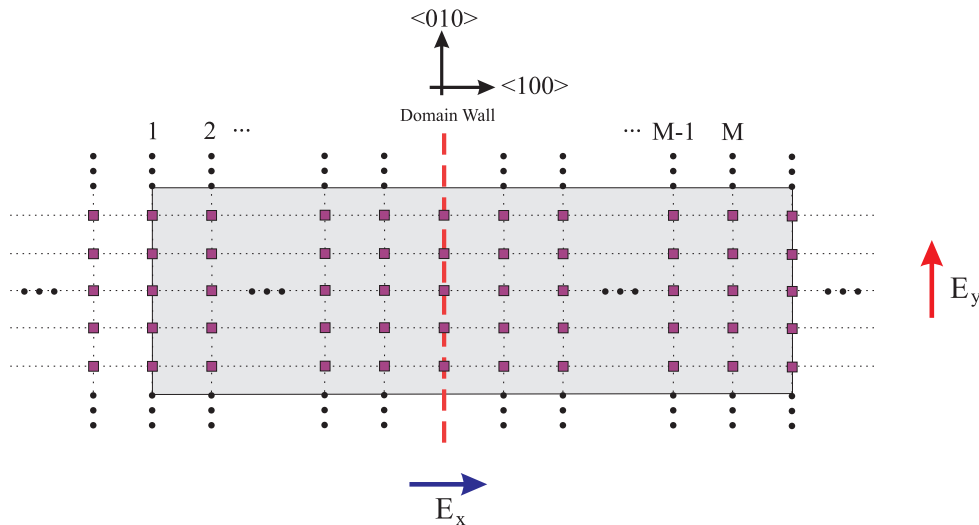


FIG. 2: Ti-cores under external electric field in a Ti-centered 180° domain wall. E_x and E_y are the normal and parallel electric fields, respectively. The shaded region denotes the region that is relaxed in each step. Note that M is the size of the computational box (CB) normal to the domain wall. We consider different CBs with one, four, and sixteen unit cells in the domain wall plane.

boundary condition as we expect the bulk configuration far from the domain wall.

In our calculations we use $M = 20$ as larger values for M do not affect the results. Imposing an external electric field should be done step by step, i.e., one first needs to obtain the configuration for $\mathbf{E} = \Delta\mathbf{E}_1$ from the initial configuration and then use this configuration to obtain the equilibrium configuration for $\mathbf{E} = \Delta\mathbf{E}_1 + \Delta\mathbf{E}_2$ and so on. We use the average step size of $20kV/cm$ for electric field. Using this step size and force tolerance of $0.005eV\text{\AA}^{-1}$, our solutions converge after about 30 to 40 iterations.

IV. NUMERICAL RESULTS

In this section we present our numerical results for perfect and defective domain walls. Note that as the coordinates of cores and shells are close to each other, we only report the results for cores. Also as we mentioned earlier, x , y , and z are coordinates along the $\langle 100 \rangle$, $\langle 010 \rangle$, and $\langle 001 \rangle$ -directions, respectively.

Perfect domain walls: We plot the y -coordinates of Ti-cores under external electric field normal to the Ti-centered domain wall, E_x , in Fig.3(a). As expected, we see that increasing the electric field, the atomic structure loses its symmetry. We observe that there exists an upper bound for E_x , i.e., there exists a critical electric field E_x^c such that for $E_x > E_x^c$ there is no local equilibrium structure. The critical value of the normal electric field is about $E_x^c = 1400kV/cm$. The thickness of the domain wall slightly increases as the normal electric field increases. Note that domain wall thickness cannot be defined uniquely very much like boundary layer thickness

in fluid mechanics. Here, domain wall thickness is by definition the region that is affected by the domain wall, i.e. those layers of atoms that are distorted. One can use definitions like the 99%-thickness in fluid mechanics and define the domain wall thickness as the length of the region that has 99% of the far field rigid translation displacement. What is important here is that no matter what definition is chosen, domain wall “thickness” increases as the normal electric field increases. For a Ti-centered domain wall, the domain wall thickness increases from 3 atomic spacings ($1nm$) to about 5 atomic spacings ($1.5nm$) for $E_x = E_x^c$.

Fig.3(b) depicts the y -coordinates of Ti-cores under an external electric field E_y parallel to a Ti-centered domain wall. It is observed that such electric fields do not alter the domain wall thickness. Note that similar to the atomic structure for normal fields, the atomic structure under parallel fields loses its symmetry as well. The critical value of the parallel electric field is about $E_y^c = 5900kV/cm$, which is 4 times larger than that of the normal electric field.

Fig.3(c) shows the y -coordinates of Pb-cores of a Pb-centered domain wall under normal electric field E_x . We observe that the critical electric field is about $E_x^c = 6300kV/cm$, which is about 4.5 times greater than the critical normal electric field of Ti-centered walls. Also it is observed that domain wall thickness increases to about 11 atomic spacings ($4nm$) under critical normal electric field. The y -coordinates of Pb-cores of a Pb-centered domain wall under parallel electric field E_y are shown in Fig.3(d). Similar to perfect Ti-centered domain walls, we observe that parallel electric fields do not affect the domain wall thickness. The critical parallel electric field is about $E_y^c = 6500kV/cm$. For Pb-centered domain walls we see that unlike Ti-centered domain walls, the critical

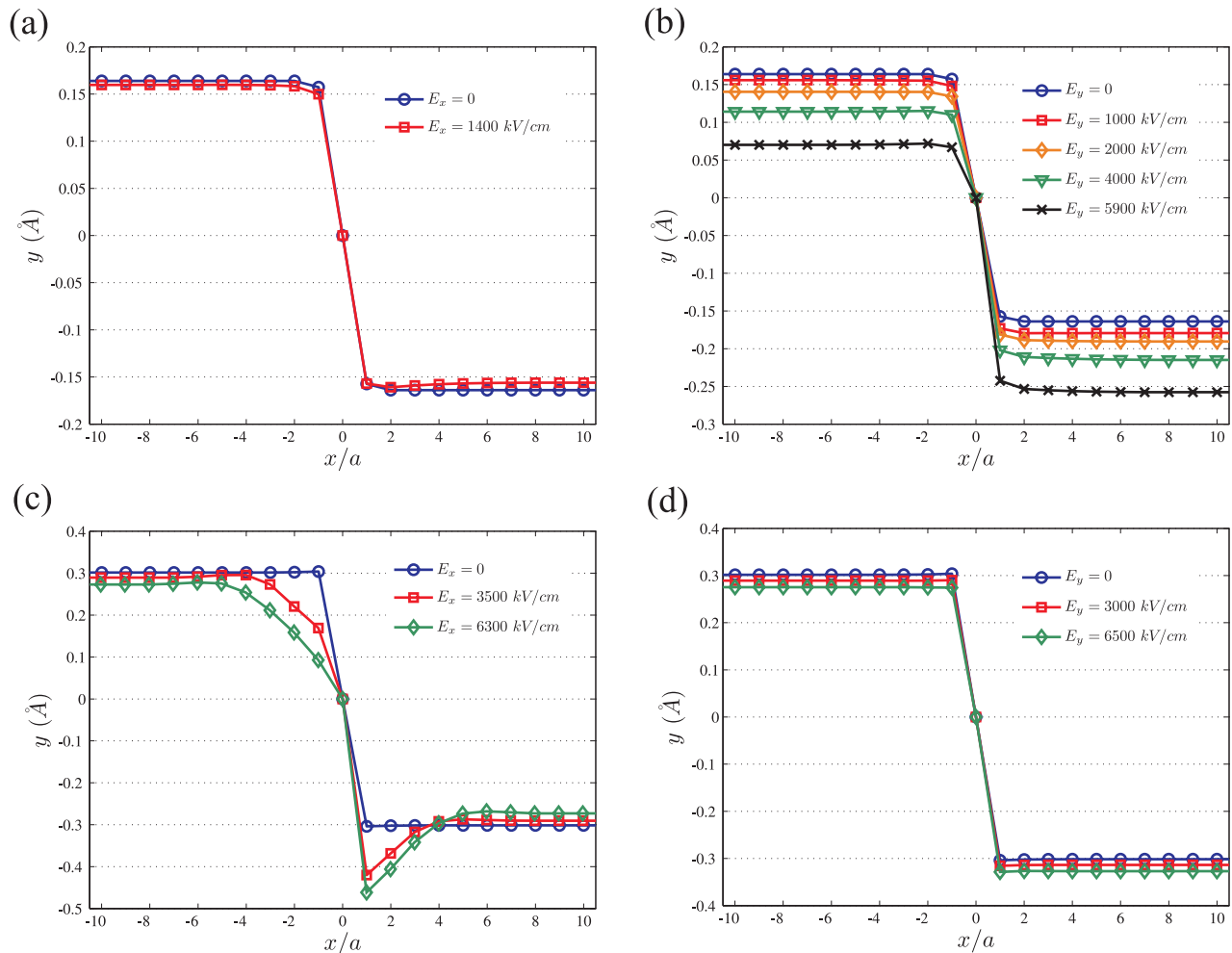


FIG. 3: The y-coordinates of cores under external electric field: Ti cores in a perfect Ti-centered domain wall under (a) E_x and (b) E_y ; Pb cores in a perfect Pb-centered domain wall under (c) E_x and (d) E_y .

normal electric field is close to the critical parallel electric field.

Fig.4 depicts the polarization profiles normal and parallel to the domain walls. For calculation of the cell-by-cell polarization, we follow Meyer and Vanderbilt⁴. We plot $\bar{\mathbf{P}} = (\bar{P}_x, \bar{P}_y) = \mathbf{P}/|\mathbf{P}_b|$, where \mathbf{P} is the polarization and $|\mathbf{P}_b| = 80.1\mu Ccm^{-2}$ is the norm of the bulk polarization²⁴. Fig.4(a) shows \bar{P}_x and \bar{P}_y for a Ti-centered domain walls under zero and critical electric fields. In agreement with Lee *et al.*²⁵ and Angoshtari and Yavari⁷, it is observed that (100) Ti-centered domain walls have a mixed Ising-Néel character, i.e., polarization rotates normal to the (100)-plane near the domain wall. For $E = 0$, the maximum normal component of the polarization is about 2% of the bulk polarization. For $E = E_x^c$, as can be expected, normal electric field causes the positive and negative charges to have normal displacements that create a polarization in the x-direction. This normal component of the polarization (\bar{P}_x) reaches to about 13.5% of the bulk polarization at E_x^c , but we observe that normal electric field E_x^c does not have a remarkable ef-

fect on the parallel component of polarization, \bar{P}_y . On the other hand, we observe that under $E = E_y^c$, \bar{P}_x does not change considerably but \bar{P}_y has an unsymmetric profile with the maximum value of about 105% of the bulk polarization.

Fig.4(b) presents similar results for Pb-centered domain walls. Similar to Ti-centered domain walls, we observe that Pb-centered domain walls have a mixed Ising-Néel character^{7,25} with \bar{P}_x about 2% of the bulk polarization for zero electric field. For $E = E_x^c$, \bar{P}_x reaches to about 38% of the bulk polarization. Also we observe that E_x^c has more impact on \bar{P}_y compared to Ti-centered walls. Finally, it is observed that similar to Ti-centered domain walls, E_y^c does not have a significant effect on \bar{P}_x but makes \bar{P}_y unsymmetric with maximum value of about 107% of the bulk polarization.

Defective domain walls: In this part we report the structure of defective domain walls under normal and parallel external electric fields. Because the results for O1- and O3-defective domain walls are similar, we only present the results for O1-defective walls, which are Ti-

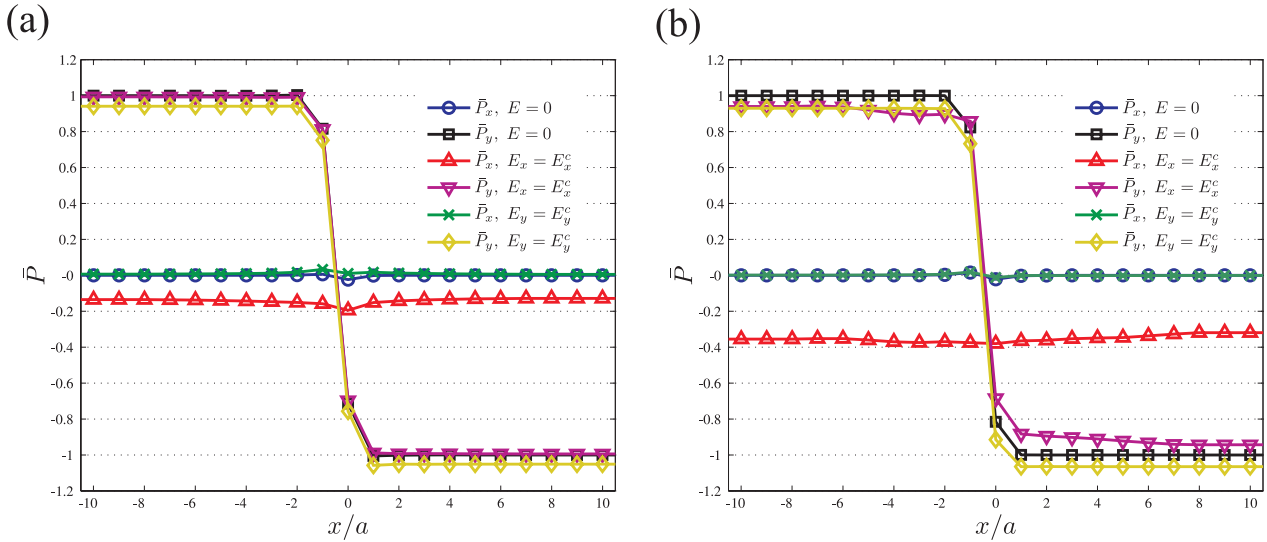


FIG. 4: The polarization profiles $\bar{\mathbf{P}} = (\bar{P}_x, \bar{P}_y)$ of domain walls under zero, normal critical field (E_x^c), and parallel critical field (E_y^c) for (a) Ti-centered, and (b) Pb-centered domain walls.

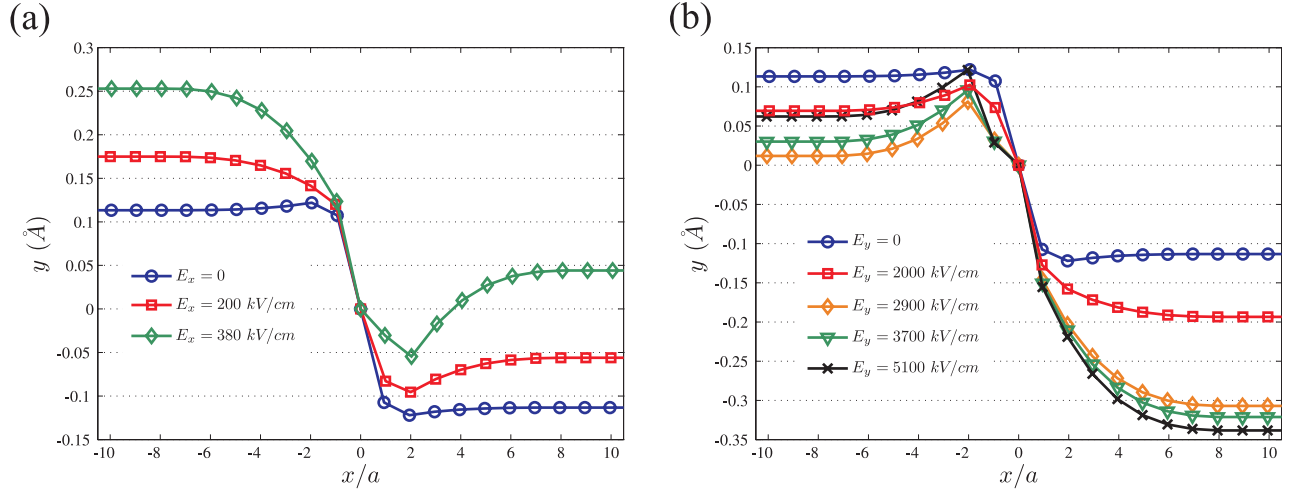


FIG. 5: The y-coordinates of Ti cores in an O1-defective domain wall under (a) normal (E_x), and (b) parallel (E_y) external electric fields.

centered. Note that as we mentioned earlier, O2-defective domain walls, which are Pb-centered, are not stable. Our calculations show that they are not stable even under external electric fields. We had earlier shown that they are not stable under strain as well¹⁸.

Fig.5(a) depicts the y-coordinates of Ti-cores in an O1-defective domain wall under normal external electric field E_x . The critical normal field is about $E_x^c = 380$ kV/cm. It is observed that domain wall thickness increases up to about 16 atomic spacings (6nm) under the critical normal electric field. Comparing O1-defective atomic structure with the structure of perfect Ti-centered domain wall under normal field (Fig.3(a)), we observe that oxygen vacancies increase the thickness of the domain wall considerably. Also it is observed that critical normal electric field of defective domain walls is smaller than that of per-

fect Ti-centered wall. Fig.5(b) shows the y-coordinates of Ti-cores in an O1-defective domain walls under parallel electric field E_y . The value of the critical field is about $E_y^c = 5100$ kV/cm. Here we observe a major difference between the atomic structures of perfect and defective domain walls; unlike perfect domain walls, parallel electric fields increase the thickness of defective domain walls up to about 13 atomic spacings (5nm) under the critical parallel electric field. Also similar to normal electric fields, we observe that critical electric field of defective domain walls is smaller than that of perfect domain walls.

Defective domain walls are thicker than perfect domain walls. The observation that the defective domain walls have smaller critical electric fields is in agreement with the experimental observations of Choudhury *et al.*¹⁰. They observed that the threshold field for domain wall

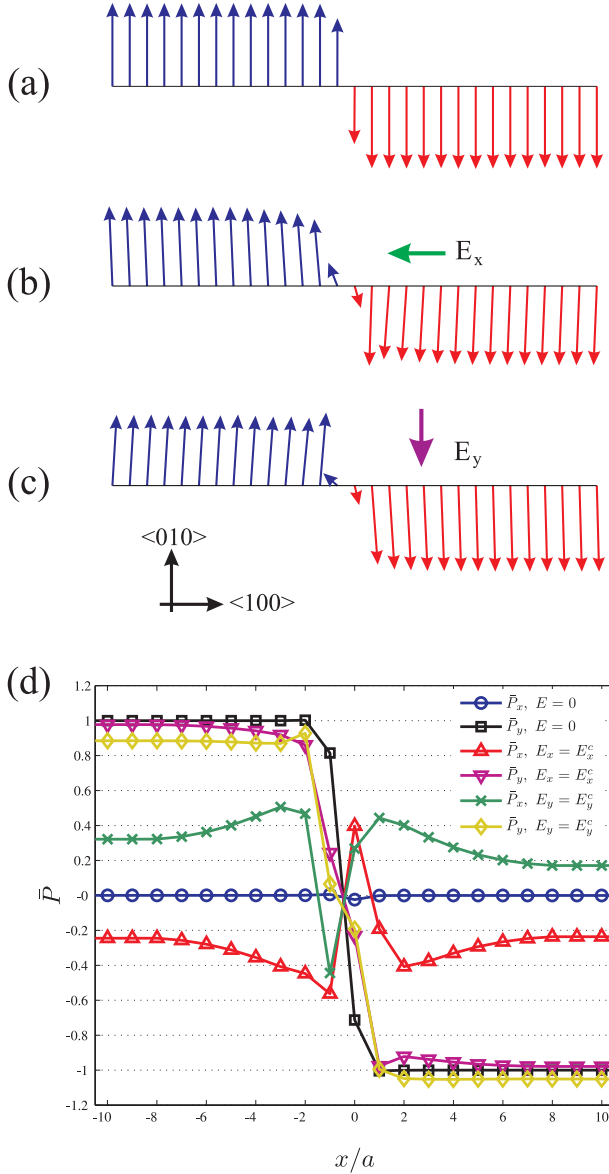


FIG. 6: The polarization profiles of O1-defective domain walls under (a) zero, (b) normal critical field (E_x^c), and (c) parallel critical field (E_y^c). (d) Components of the polarization vector $\bar{\mathbf{P}} = (\bar{P}_x, \bar{P}_y)$ of O1-defective domain walls under zero, E_x^c , and E_y^c .

motion exponentially decreases as the domain wall width increases.

Fig.6 shows the polarization profiles for O1-defective domain walls. It is observed that similar to perfect domain walls, defective domain walls have an Ising-Néel character with \bar{P}_x of about 2.5% of the bulk polarization for zero electrical field. For $E = E_x^c$, \bar{P}_x reaches to about 55% of the bulk polarization, which is greater than the corresponding values for perfect domain walls, and \bar{P}_y shows more Ising-type character. As we mentioned ear-

lier, for $E = E_y^c$ we observe a difference between perfect and defective domain walls; unlike perfect walls, parallel electric fields have considerable effects on \bar{P}_x : it reaches to about 55% of the bulk polarization under E_y^c . Similar to perfect domain walls, \bar{P}_y has an unsymmetric distribution and reaches to about 106% of the bulk polarization.

V. CONCLUDING REMARKS

In this work we obtained the atomic structure of perfect and defective 180° domain walls in PbTiO_3 under both parallel and normal external electric fields using the method of anharmonic lattice statics. We observe that electric field can increase the thickness of a domain wall considerably (up to 5 times thicker than domain walls under no external electric field). This can be one reason for the wide scatter of the domain wall thicknesses observed in experimental measurements. In agreement with previous works^{11,18}, we observe that oxygen vacancies can increase the thickness of the domain walls. We also observe that by increasing the external electric field we reach a critical electric field E^c . For $E > E^c$ there is no local equilibrium configuration and hence E^c can be considered as an estimate of the threshold field for the domain wall motion. We observe that defective domain walls, which are thicker than perfect domain walls, have smaller critical fields. This is in agreement with the experimental observations that show the threshold field decreases as the domain wall thickness increases¹⁰.

In practice, it has been observed that domain walls move or break down under electric fields in the order of a few kV/cm ^{10,26}, which are considerably smaller than the high-fields that we consider here. We do not consider break down of the domain walls in our model. Also as was mentioned earlier, the high density of oxygen vacancies that we assume is unrealistic. In practice, steps and other complex defects on domain walls can increase the thickness of the domain walls considerably^{8,9,24}. Therefore, as the threshold fields for domain walls decrease exponentially with the increase of the domain wall width¹⁰, one can obtain better estimates for the critical electric fields with more realistic models for defects on domain walls. Also as suggested by Roy *et al.*²⁶ electric fields change the potential parameters. In this paper our aim is to demonstrate that even with our simple model, one can show that the threshold field has an inverse relation with the domain wall thickness.

Acknowledgments

We benefited from a discussion with C.M. Landis. We thank an anonymous reviewer whose comments helped us improve the paper.

-
- * Electronic address: arash.yavari@ce.gatech.edu
- ¹ J. F. Scott, *Science*, **315**, 954 (2007).
 - ² S. V. Kalinin, A. N. Morozovska, L. Q. Chen and B. J. Rodriguez, *Rep. Prog. Phys.*, **73**, 056502 (2010).
 - ³ C-L. Jia, S-B. Mi, K. Urban, I. Vrejoiu, M. Alexe, D. Hesse, *Nature Mater.*, **7**, 57 (2008).
 - ⁴ B. Meyer and D. Vanderbilt *Phys. Rev. B*, **65**, 104111 (2002).
 - ⁵ J. Padilla, W. Zhong and D. Vanderbilt *Phys. Rev. B*, **53**, R5969 (1996).
 - ⁶ A. Yavari, M. Ortiz and K. Bhattacharya, *Philos. Mag.*, **87**, 3997 (2007).
 - ⁷ A. Angoshtari and A. Yavari, *EPL*, **90**, 27007 (2010).
 - ⁸ M. Iwata, K. Katsuraya, I. Suzuki, M. Maeda, N. Yasuda and Y. K. Ishibashi, *Jpn. J. Appl. Phys.*, **42**, 6201 (2003).
 - ⁹ P. Lehnen, J. Dec and W. Kleemann, *J. Phys. D: Appl. Phys.*, **33**, 1932 (2000).
 - ¹⁰ S. Choudhury et al., *J. Appl. Phys.*, **104**, 084107 (2008).
 - ¹¹ D. Shilo, G. Ravichandran and K. Bhattacharya, *Nature Mater.*, **3**, 453 (2004).
 - ¹² W. T. Lee, E. K. H. Salje and U. Bismayer, *Phys. Rev. B*, **72**, 104116 (2005).
 - ¹³ A. K. Bandyopadhyay and P. C. Ray, *J. Appl. Phys.*, **95**, 226 (2004).
 - ¹⁴ Y. Su and C. M. Landis, *J. Mech. Phys. Solids*, **55**, 280 (2007).
 - ¹⁵ L. X. He and D. Vanderbilt, *Phys. Rev. B*, **68**, 134103 (2001).
 - ¹⁶ M. Calleja, M. T. Dove and E. K. H. Salje, *J. Phys.: Condens. Matter*, **15**, 2301 (2003).
 - ¹⁷ L. Goncalves-Ferreira, S. A. T. Redfern, E. Artacho, E. Salje and W. T. Lee, *Phys. Rev. B*, **81**, 024109 (2010).
 - ¹⁸ A. Angoshtari and A. Yavari, *Comput. Mater. Sci.*, **48**, 258 (2010).
 - ¹⁹ A. Yavari, M. Ortiz and K. Bhattacharya, *J. Elasticity*, **86**, 41 (2007).
 - ²⁰ A. Yavari and A. Angoshtari, *Inter. J. Solids Struct.*, **47**, 1807 (2010).
 - ²¹ A. Asthagiri, Z. Wu, N. Choudhury and R. E. Cohen, *Ferroelec.*, **333**, 69 (2006).
 - ²² D. P. Wolf, P. Keblinski, S. R. Phillpot and J. Eggebrecht, *J. Chem. Phys.*, **110**, 8254 (1999).
 - ²³ W. H. Press, S. A. Teukolsky, W. T. Vetterling, and B. P. Flannery, *Numerical recipes: the art of scientific computing* (Cambridge University Press, Cambridge, 1989).
 - ²⁴ A. Angoshtari and A. Yavari, *J. Appl. Phys.*, **108**, 084112 (2010).
 - ²⁵ D. Lee, R. K. Behera, P. Wu, H. Xu, Y. L. Li, S. B. Sinnott, S. R. Phillpot, L. Q. Chen and V. Gopalan, *Phys. Rev. B*, **80**, 060102(R) (2009).
 - ²⁶ A. Roy, M. Stengel, and D. Vanderbilt, *Phys. Rev. B*, **81**, 014102 (2010).